MODELLING THE EFFECT OF ACTIVE FLOW CONTROL VIA PULSATION ON TURBULENT FLOW IN A 10° PLANE DIFFUSER

Tim J. Craft, Hector Iacovides, Parham Momeni
Turbulence Mechanics Group
School of Mechanical, Aerospace and Civil Engineering
The University of Manchester
Manchester M60 1QD, UK
Email: Parham_momeni@hotmail.com

ABSTRACT

In recent years there has been considerable interest in the active control of fluid flow phenomena. Applications include separation control, drag reduction and lift enhancement. The present study is concerned with flow separation and reattachment, and considers the case of flow through a 10° plane diffuser, studied experimentally by Masuda et al (1994), where the control is provided by a periodic injection/suction upstream of where the flow would separate under stationary conditions.

Results are reported using the two-equation linear k-ε model of Launder & Sharma (1974) and a two-equation non-linear k-ε scheme (Craft et al., 2005), in conjunction with the Reynolds-averaged momentum (URANS) equations. The linear scheme does not capture the flow separation in the unforced case, whilst the non-linear model does better, although slightly underpredicts the recirculation zone size. In the unsteady, forced, cases the non-linear scheme generally reproduces the effect of the forcing in enhancing the coherence of the separated shear layers and reducing the reattachment length at the lower forcing frequencies, whilst showing a smaller effect as the frequency is increased.

INTRODUCTION

During the past two decades, there has been considerable attempt to develop methodologies and tools to actively control fluid flow phenomena. Applications include separation control, drag reduction, lift enhancement, and virtual aerodynamic shaping. Of particular interest here are flows involving separation and reattachment, which are found in a range of engineering systems including vehicles and planes.

The test case examined is that of flow through a 10° plane diffuser, studied experimentally by Masuda et al (1994), as shown in Figure 1. The control is provided by an imposed pulsation from a periodic injection/suction upstream of where the flow would separate under stationary conditions. Since the separation point here is not geometrically fixed, the control affects both the flow detachment and reattachment processes, and this poses significant challenges in the computational modelling.

Computing flows exhibiting even steady detachment and reattachment is by no means a trivial task, and in order to minimise computing times there is a desire to employ relatively simple RANS models of turbulence. Linear eddy-viscosity models (LEVM's) are, however, known to perform badly in separated flows. Craft et al (2005) introduced refinements to a low-Reynolds-number non-linear eddy-viscosity model (NLEVM) and showed that this performed quite successfully in predicting the steady flow and heat transfer through a sudden pipe expansion. Craft et al (2007) subsequently applied this model to periodically forced flows through a pipe expansion. The overall effect of the forcing, namely a reduction in the size of the separation zone, together with a more intense back flow, was captured by the model and, as a result, the time-averaged heat transfer profiles showed higher levels in the separated region and a peak which was further upstream than in the steady flow case.

The objectives of the present study are thus to establish how well the above non-linear model can perform in the case of the 10° diffuser, where neither separation nor reattachment is fixed by the geometry, and to use the computed results to advance our understanding of the mechanisms of flow control with pulsation.

The following sections outline the modelling approaches tested, describe the flow cases considered, and present comparisons between the model predictions and available experimental data.

MODELLING APPROACH

Two-Equation Linear *k-ε* Model:

The simplest model employed in this study is the linear k-ε scheme of Launder & Sharma (1974), which approximates the turbulent stresses and heat fluxes by

$$\overline{u_i u_j} = \frac{2}{3} k \, \delta_{ij} - v_t \left(\frac{\partial U_i}{\partial x_j} + \frac{\partial U_j}{\partial x_i} \right) \qquad (1)$$

where the turbulent viscosity $v_t = c_\mu \, f_\mu \, k^2 / \tilde{\varepsilon}$ and k and $\tilde{\varepsilon}$ are obtained from the transport equations

$$\frac{Dk}{Dt} = \frac{\partial}{\partial x_j} \left(\left(v + \frac{v_t}{\sigma_k} \right) \frac{\partial k}{\partial x_j} \right) + P_k - \varepsilon \qquad (2)$$

$$\frac{D\tilde{\varepsilon}}{Dt} = \frac{\partial}{\partial x_j} \left(\left(v + \frac{v_t}{\sigma_{\tilde{\varepsilon}}} \right) \frac{\partial \tilde{\varepsilon}}{\partial x_j} \right)$$
$$+ C_{\varepsilon 1} \frac{P_k \tilde{\varepsilon}}{k} - C_{\varepsilon 2} f_2 \frac{\tilde{\varepsilon}^2}{k} + E + Y_{dc} \qquad (3)$$

where $\varepsilon = \tilde{\varepsilon} + 2v \left(\partial k^{0.5} / \partial x_j \right)^2$.

The production rate of turbulent kinetic energy, P_k, is given by

$$P_k = -\overline{u_i u_j} \frac{\partial U_i}{\partial x_j} \quad (4)$$

whilst E is the near-wall source term

$$E = 2 v \, v_t \left(\frac{\partial^2 U_i}{\partial x_j \partial x_k} \right)^2 \quad (5)$$

The term Y_{dc} is the lengthscale correction originally proposed by Raisee (1999), and subsequently re-tuned by Craft et al. (2005), which is based on lengthscale gradients, and can be written as

$$Y_{dc} = C_w \frac{\tilde{\varepsilon}^2}{k} \max\left[F^{0.4} (F+1)^2, 0 \right] \quad (6)$$

where F essentially measures the difference between the predicted lengthscale gradient and the value it would take in an equilibrium boundary layer:

$$F = \frac{1}{C_l} \left\{ \left[\left(\frac{\partial l}{\partial x_j} \right) \left(\frac{\partial l}{\partial x_j} \right) \right]^{0.5} - dl_e / dy \right\} \quad (7)$$

with $l = (k^{1.5} / \varepsilon)$ and the term dl_e / dy standing for the equilibrium lengthscale gradient, given by:

$$C_l [1 - \exp(-B_\varepsilon \tilde{R}_t)] + B_\varepsilon C_l \tilde{R}_t \exp(-B_\varepsilon \tilde{R}_t) \quad (8)$$

The various model coefficients and near-wall damping terms are given in Table 1, whilst $\tilde{R}_t$ is the turbulent Reynolds number, $\tilde{R}_t = k^2 / (\tilde{\varepsilon} v)$.

Two-Equation Non-Linear *k-ε* Model:

The above linear EVM is known to have many weaknesses, so much of the present work has been carried out within the framework of non-linear eddy-viscosity models. The form adopted here is that proposed by Craft et al (2005), which was developed from the earlier versions of Craft et al. (1999) and Suga (1996). In this scheme, the Reynolds stresses are approximated by

$$\overline{u_i u_j} = (2/3) k \delta_{ij} - v_t S_{ij}$$
$$+ C_1 \frac{v_t}{\tilde{\varepsilon}} k \left(S_{ik} S_{jk} - (1/3) S_{kl} S_{kl} \delta_{ij} \right)$$
$$+ C_2 \frac{v_t}{\tilde{\varepsilon}} k \left(\Omega_{ik} S_{jk} + \Omega_{jk} S_{ik} \right)$$
$$+ C_3 \frac{v_t}{\tilde{\varepsilon}} k \left(\Omega_{ik} \Omega_{jk} - (1/3) \Omega_{kl} \Omega_{kl} \delta_{ij} \right) \quad (9)$$
$$+ C_4 \frac{v_t k^2}{\tilde{\varepsilon}^2} \left(S_{ki} \Omega_{lj} + S_{kj} \Omega_{li} \right) S_{kl}$$
$$+ C_6 \frac{v_t k^2}{\tilde{\varepsilon}^2} \left(S_{ij} S_{kl} S_{kl} \right) + C_7 \frac{v_t k^2}{\tilde{\varepsilon}^2} \left(S_{ij} \Omega_{kl} \Omega_{kl} \right)$$

Table 1: Coefficients and damping functions in the linear k-ε model.

σ_k , $\sigma_{\tilde{\varepsilon}}$	1 , 1.3
f_2	$1 - 0.3 \exp\left(-\tilde{R}_t^2 \right)$
c_μ , f_μ	0.09 , $\exp\left(\dfrac{-3.4}{(1 + \tilde{R}_t / 50)^2} \right)$
C_l, B_ε, C_w	2.55 , 0.1069 , 083
$C_{\varepsilon 1}, C_{\varepsilon 2}$	1.44 , 1.92

where S_{ij} and Ω_{ij} are the strain and vorticity tensors, defined as

$$S_{ij} = \left(\frac{\partial U_i}{\partial x_j} + \frac{\partial U_j}{\partial x_i} \right), \quad \Omega_{ij} = \left(\frac{\partial U_i}{\partial x_j} - \frac{\partial U_j}{\partial x_i} \right) \quad (10)$$

In modelling the turbulent eddy viscosity, the quantities f_μ and c_μ are taken as

$$f_\mu = f_{\mu i} f_s + (1 - f_s) \quad (11)$$

with

$$f_{\mu i} = 1 - \exp\left(-\left(\tilde{R}_t / 90\right)^{0.5} - \left(\tilde{R}_t / 400\right)^2 \right) \quad (12)$$

$$f_s = \min\left(\frac{\max\left((P_k / \tilde{\varepsilon}) \min\left(1, \tilde{R}_t / 50\right)^2, 0 \right)}{0.75}, 1 \right) \quad (13)$$

and

$$c_\mu = \min\left[0.09, \frac{1.2}{1 + \alpha \eta + f_{RS}} \right] \quad (14)$$

where

$$\eta = \max (\tilde{S}, \tilde{\Omega}) \quad (15)$$

with

$$\alpha = 3.5 - 0.5 \left(1 - \exp\left(-\left(\tilde{R}_t / 400\right)^2 \right) \right) \quad (2)$$

and

$$f_{RS} = 0.235 \left[\max(0, \eta - 3.333) \right]^2 \exp(-\tilde{R}_t / 400) \quad (3)$$

$$\tilde{S} = \frac{k}{\tilde{\varepsilon}} \sqrt{\frac{(S_{ij} S_{ij})}{2}}, \quad \tilde{\Omega} = \frac{k}{\tilde{\varepsilon}} \sqrt{\frac{(\Omega_{ij} \Omega_{ij})}{2}} \quad (18)$$

The remaining model coefficients are given in Table 2.

The $\tilde{\varepsilon}$ equation is similar to that employed in the Launder-Sharma model, but the near-wall source term E is replaced by

$$E = \begin{cases} 0.0022 \dfrac{v_t \tilde{S} k^2}{\tilde{\varepsilon}} \left(\dfrac{\partial^2 U_i}{\partial x_j \partial x_k} \right)^2 & \tilde{R}_t \le 250 \\ 0 & \tilde{R}_t > 250 \end{cases} \quad (19)$$

Table 2 : Coefficients in the two-equation cubic stress-strain relation.

C_1	C_2	C_3	C_4	C_6	C_7
-0.1	0.1	0.26	$-10\,c_\mu^2$	$-5\,c_\mu^2$	$5\,c_\mu^2$

and the coefficient employed in the lengthscale correction Y_{dc} in equation (7) is modified as

$$C_w = \frac{\left\{ 3.4\,(1-f_s)\left(\min\,(1,\tilde{R}_t/25)\right)^2 \right\}}{[0.8 + 0.7\,(\eta'/3.33)^4 \exp(-\tilde{R}_t/12.5)]} + \frac{\left\{ 0.75\,f_s\,\min\,(1,\tilde{R}_t/40) \right\}}{[0.8 + 0.7\,(\eta'/3.33)^4 \exp(-\tilde{R}_t/12.5)]} \quad (20)$$

where the quantity η' is defined as $\eta' = \max\,(\tilde{S}',\tilde{\Omega}')$

and $\tilde{S}'$ and $\tilde{\Omega}'$ are taken as

$$\tilde{S}' = \left(\max\left[\frac{k}{\tilde{\varepsilon}}, \sqrt{\frac{v}{\tilde{\varepsilon}}} \right] \right)\sqrt{\frac{1}{2}\,S_{ij}\,S_{ij}}$$

$$(21)$$

$$\tilde{\Omega}' = \left(\max\left[\frac{k}{\tilde{\varepsilon}}, \sqrt{\frac{v}{\tilde{\varepsilon}}} \right] \right)\sqrt{\frac{1}{2}\,\Omega_{ij}\,\Omega_{ij}}$$

CASE STUDIED

The test case examined is that studied experimentally by Aoki et al. (1993) (under steady state conditions) and Masuda et al. (1994) (with an imposed unsteady jet as flow control). As shown in Figure 1, it consists of flow through a 10° plane diffuser with a span-wise slit on the diffuser wall, located upstream of the detachment point. The perturbation is accomplished by periodically alternating between flow suction and injection through this slit. The experiment without flow control has proved useful and popular for assessing turbulence models, due to the smooth-wall flow separation which occurs. The diffuser angle is not so large as to cause separation of the flow on entry to the diffuser, yet it is large enough to generate an adverse pressure gradient which will cause a turbulent flow to separate. Separation from the inclined wall occurs at about one-third of the distance along the diffuser.
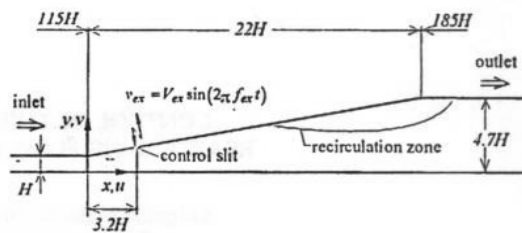
Figure 1: Schematic of the test section of the experiment of Masuda et al (1994).

The Reynolds number based on upstream channel height and bulk velocity was $Re_b = 20000$, the same as used by Aoki et al. (1993) and Masuda et al. (1994) in their experiments. In these experiments, the flow at the inlet of the diffuser was fully developed. This was reproduced for the present calculations by a pre-calculation of flow between parallel plates using periodic inlet and outlet boundaries. This provided fully-developed profiles of the velocity and the Reynolds stresses for the inlet of the main calculation (a separate pre-calculation was made for each turbulence model).

The flow forcing is introduced by periodically alternating flow suction and injection through a span-wise slit on the diffuser wall. This slot, of width $g=0.1H$ (H being the inlet channel height), is located at $X/H=3.2$. The jet velocity here is assumed to have a uniform spatial profile, but varies sinusoidally in time as

$$U_j(t) = A\,U_0 \sin(2\pi f\,t) \quad (22)$$

where $A=0.3$ is defined as the forcing amplitude, and a range of frequencies, $0.01 < St_H < 0.2$ (where the Strouhal number $St_H = fH/U_o$) have been studied.

In the results below, comparisons are drawn between the time and phase-averaged predictions and available experimental data. Most computations have employed the non-linear EVM, although some comparisons are also shown for the linear Launder-Sharma scheme.

NUMERICAL IMPLEMENTATION

The computations have been performed using an in-house FORTRAN code (STREAM), based on a finite-volume scheme with a fully collocated grid storage arrangement. The pressure-velocity coupling is handled by the SIMPLE scheme, and second order schemes for both spatial (UMIST) and time (Crank-Nicolson) discretisation have been employed. In all the unsteady cases the simulations were run for a large number of cycles before data was collected, so that the results presented correspond to fully-periodic conditions.

Since low-Reynolds-number models are used in the present study, the grid must be fine enough to capture the gradients that occur near the wall. Grid and time-step sensitivity tests were performed, and the results reported below, using a non-uniform grid of 320x100 cells and 6000 timesteps to cover an injection/suction cycle, can be considered essentially grid and time-step independent.

RESULTS

For flows over geometries where separation is not fixed by sharp corners, predicting the correct location of the separation line depends on modelling the correct response of the shear stress, and to some degree also the normal stresses, to deceleration; that is, of predicting the correct turbulent time scale. Beyond the separation point, the flow loses much of the direction-constraining influence of the boundary, and all components of the Reynolds-stress tensor become significant. At the same time, the rate of recovery and, hence, the reattachment point, depend on the magnitude of the shear stress in a (curved) free shear layer. The challenges for turbulence models in such a flow are,

therefore, (i) to predict the correct turbulent time scale in decelerated wall and free shear layers; and (ii) to predict the correct anisotropy of the Reynolds-stress tensor.

Steady State Flow Predictions

Starting with the unforced case (steady state), the computed streamlines with the LEVM and the NLEVM are compared in Figure 2. As also reported by other researchers, the linear model predicts no separation and consequently no reattachment. However, the streamlines for the non-linear model indicate that the oncoming flow separates at around $X/H=8$ (slightly later than the measured separation, $X/H=7$), and reattaches at around $X/H=24$, slightly earlier than the measured reattachment of $X/H=29$. Downstream of the reattachment point, the flow builds up a new boundary layer.

a) Linear k-ε model

b) Non-linear k-ε model
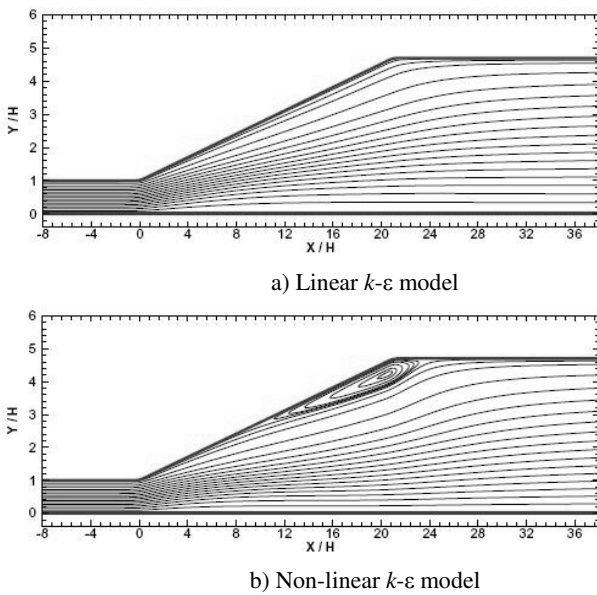
Figure 2. Streamlines of the steady flow with linear and non-linear k-ε models.

The coefficients of pressure (C_P) and skin friction (C_f) are calculated on the plane and inclined walls as follows:

$$C_p = (P - P_o)/(0.5\rho U_b^2) \qquad (4)$$

$$C_f = \tau_w/(0.5\rho U_b^2) \qquad (5)$$

where P and τ_w are the pressure and shear stress calculated at a given cell on the wall, ρ is the density (constant in these incompressible calculations), U_b is the inlet bulk velocity and P_o is the reference pressure at $X/H = -4$ and $Y/H = 0.001$. C_f is a useful indicator of flow separation, since one way of defining this is where the time-averaged value of τ_w is zero (and hence $C_f = 0$).

Coefficients of pressure and skin friction calculated by both the linear and the non-linear k-ε model on the inclined wall are shown in Figure 3. There is a clear improvement in the prediction of C_P and C_f on the inclined wall due to the use of the non-linear model in comparison to the linear model. C_P calculated by the non-linear k-ε model in the latter part of the diffuser and downstream section reproduces the measured data well and the profile of C_f confirms the separation and reattachment points reported above.

Active Flow Control Computations

In the experiment performed by Masuda et al. (1994), the influence of the perturbation on flow reattachment was examined in terms of the reverse flow fraction, γ, measured at a fixed point near the unperturbed reattachment point. γ was calculated as the ratio of the number of negative velocity samples to the total number of valid velocity signals sampled during the measurement time. Predicted values of this ratio calculated from the phase-averaged flow field versus Strouhal number ($St_H = fH/U_b$) with the non-linear k-ε model are presented in Figure 4. This definition is believed to be close, but not identical, to the definition of the experimental γ ratio. The forcing is seen to produce a maximum reduction in the γ ratio occurring over a Strouhal number range of $0.01 < St_H < 0.03$.

Another measure used here to characterize the flow is the time-averaged reattachment point, defined as the first point, starting from downstream of the diffuser and moving upstream, where the near-wall time-averaged stream-wise velocity changes sign. This is not the same as the reverse flow fraction, γ, since the latter depends only on the proportion of the total time for which the axial velocity at a position is negative, while the former is also influenced by the velocity magnitude. Figure 5 shows the variation of the reattachment point determined from the time-averaged flow field divided by its steady state predicted value, X_{rs}, with the forcing frequency. It is seen that for $0.005 < St_H < 0.03$, the forcing jet has a maximum effect on the time-averaged separation bubble size, resulting in an attached time-averaged flow. At higher frequencies the flow field returns to its steady state reattachment point prediction.
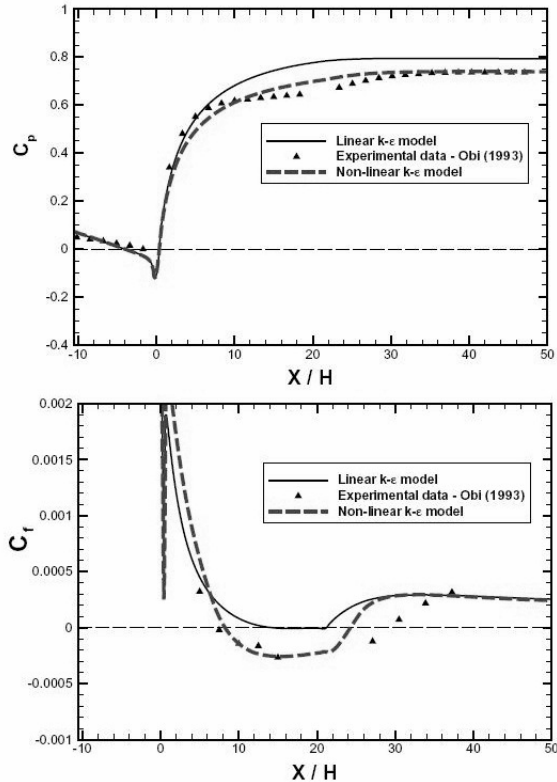
Figure 3. Coefficients of pressure (Cp) and skin friction (C_f) on the inclined wall for steady flow calculated using linear and non-linear k-ε models.
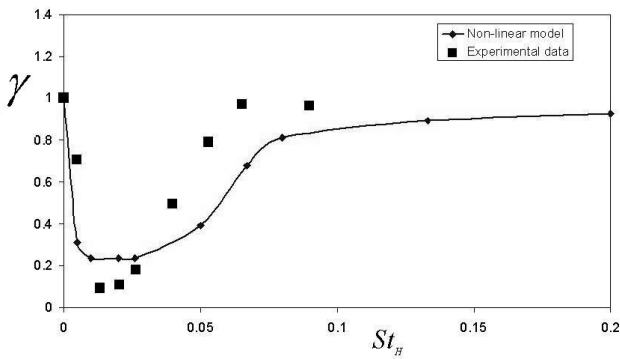
Figure 4. γ ratio versus Strouhal number with the non-linear k-ε model.
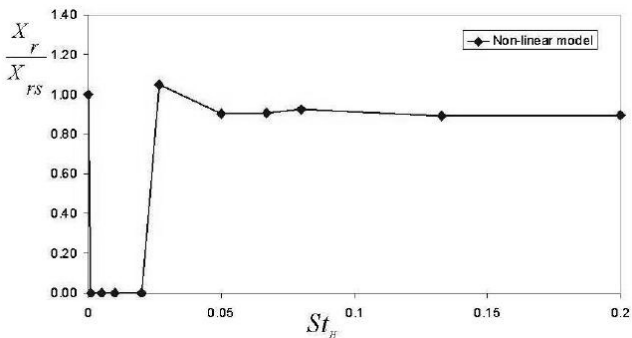
Figure 5. Normalised reattachment length of the time-averaged flow field versus Strouhal number with the non-linear k-ε model.

To further illustrate the effects of the forcing on the time-averaged flow, Figure 6 shows time-averaged coefficients of skin friction calculated with the NLEVM on the inclined wall, which indicate a substantial variation in the time-averaged flow separation zone length over the tested range of Strouhal numbers. At the lowest Strouhal number of 0.005 the time-averaged flow field does not show any recirculation, but as the Strouhal number is increased the skin friction coefficient profiles move toward the steady state prediction. It is also noted that at the lowest Strouhal number even the far downstream region of the time-averaged flow is affected, showing a slight increase of C_f compared to the other predictions.

The complexity of the phase-averaged flow field is illustrated in Figures 7 and 8, which show predicted phase-averaged streamlines and the corresponding k contours for the forced case at a Strouhal number of 0.005 at four phase times (0, $\pi/2$, π, $3\pi/2$). Although, as shown in Figure 6, the time-averaged flow field at this Strouhal number shows no separation, significantly wavy streamline patterns are shown at each phase, with a separation bubble that moves along the inclined wall during the cycle, and even a separation zone near the plane surface during part of the cycle. The phase-averaged k contours again show that the flow over most of the domain is highly affected by the imposed jet. Although not shown here, at higher frequencies the imposed perturbation decays rapidly in the downstream direction, leaving only small traces of its influence in the region of separation and recovery.
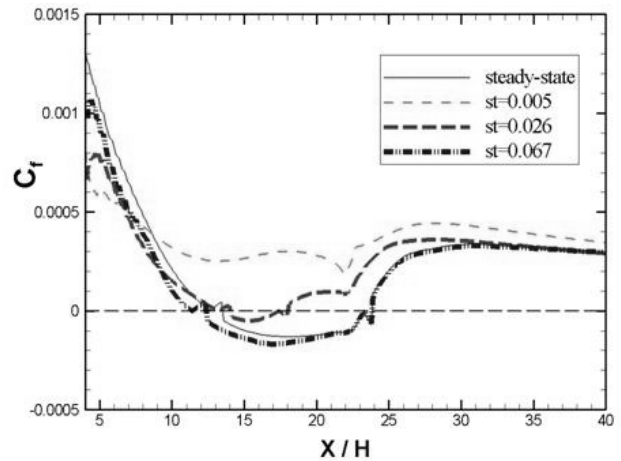
Figure 6. Time-averaged skin friction (C_f) on the inclined wall calculated using the non-linear k-ε model at $St_H = 0.005, 0.026, 0.067$
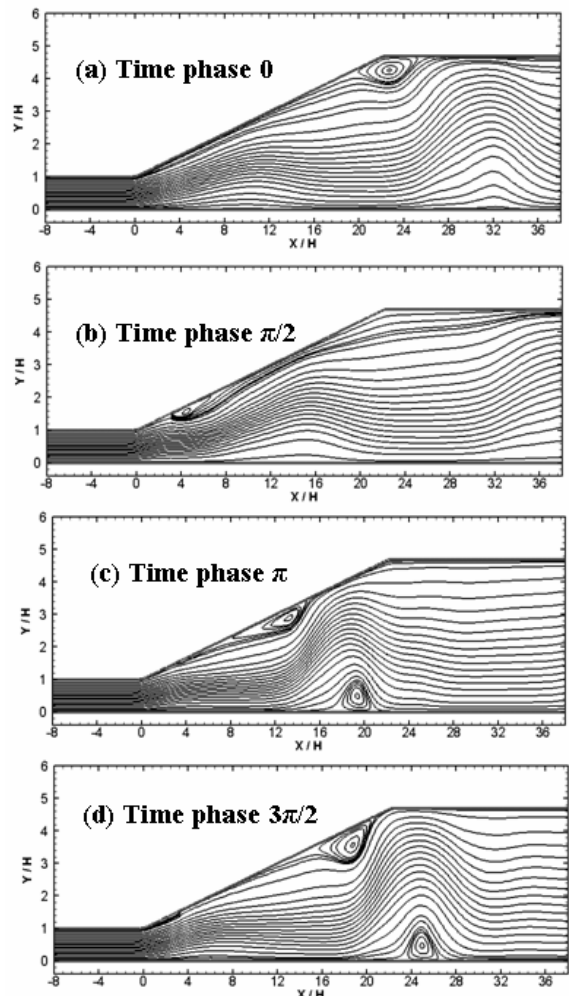
Figure 7. Phase-averaged streamlines at $St_H = 0.005$ with the non-linear k-ε model at four time phases (0, $\pi/2$, π, $3\pi/2$)
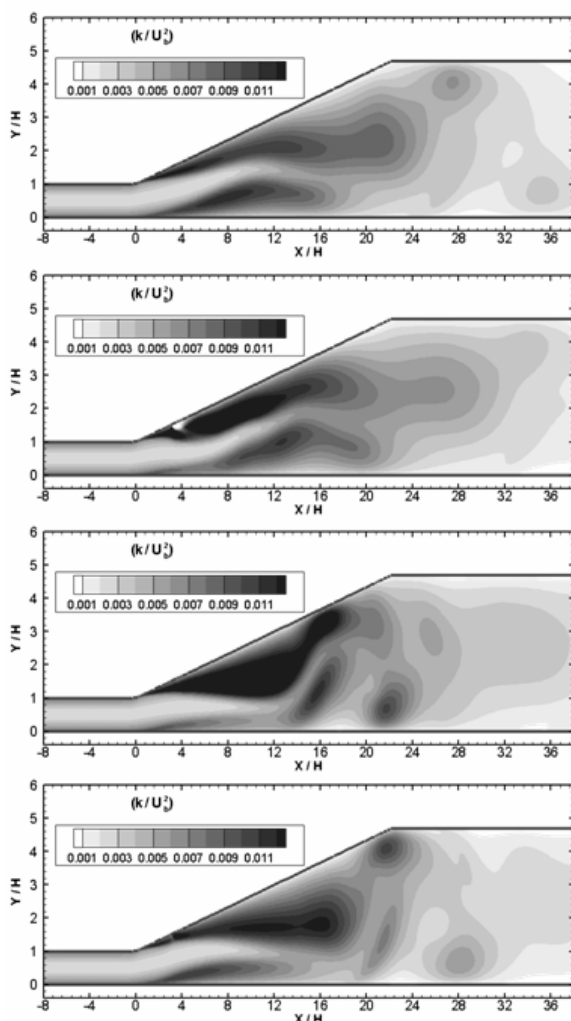
Figure 8. Phase-averaged k contours at $St_H = 0.005$ with the non-linear k-ε model at four time phases (0, $\pi/2$, π, $3\pi/2$)

As shown above, at the very low frequency of $St_H = 0.005$, most of the flow region is affected by the imposed jet. For $St_H > 0.03$, the effect of increasing Strouhal number on the oscillation of the phase-averaged flow field, when viewed in terms of the phase and amplitude characteristics of its response, was found to be a progressive reduction in the amplitude of its oscillation. At higher imposed frequencies the unsteadiness did not penetrate into the downstream region, and the flow essentially became frozen shortly beyond the jet slot.

Although not shown here, FFT results for the NLEVM predictions show that the flow disturbances mostly occur at the same frequency as the imposed perturbation for all tested Strouhal numbers.

CONCLUSIONS

Flow in a 10° plane diffuser has been used to demonstrate improvements in the flow calculation due to the non-linear k-ε model. This test case has demonstrated the relative capabilities of the linear and non-linear models to calculate smooth wall separation and reattachment in an adverse pressure gradient, and their ability to capture the effects of the imposed flow control.

Calculations with the linear k-ε model do not reproduce the unforced case well, predicting no separation on the inclined wall. The non-linear model returns improved results, although the size of the separation bubble is slightly underpredicted.

The effect of the periodic perturbation varies according to its frequency. In general, it leads to a reduction of the separation length, as a result of the enhanced momentum transport across the diffuser due to the organised oscillatory fluid motion. This effect is seen most clearly within the non-dimensional Strouhal number range of $0.005 < St_H < 0.03$. Over this range, the effect of the induced perturbation extends downstream, giving rise to oscillations of the streamlines and splitting of the instantaneous recirculation zones. At higher frequencies, the imposed perturbation decays rapidly in the downstream direction, leaving only small traces in the region of separation.

Although not shown here, both linear and non-linear k-ε models do qualitatively capture the changes in turbulent and mean velocity profile shapes. However, the non-linear model generally returns the better quantitative results, including capturing reasonably accurately the variation of the recirculation zone as the forcing frequency is changed.

REFERENCES

Aoki, K., Obi, S. and Masuda, S., (1993), Experimental and computational study of turbulent separating flow in an asymmetric plane diffuser, 9th Symposium on Turbulent Shear Flows, Kyoto, Japan.

Craft, T.J., Iacovides, H.. and Yoon, J.H., (1999), Progress in the use of non-linear two-equation models in the computation of convective heat-transfer in impinging and separated flows, Flow, Turbulence & Combustion, Vol. 63, pp. 59-80.

Craft, T.J., Iacovides, H. and Momeni, P., (2005), Computations of flow and heat transfer in abrupt pipe expansions using non-linear eddy-viscosity models of turbulence, Proc. 9th UK National Heat Transfer Conference, Manchester.

Craft, T.J., Iacovides, H. and Momeni, P., (2007), Modelling the effect of forced unsteadiness on flow and heat transfer in separated and reattaching flows, 5th International Symposium on Turbulence and Shear Flow Phenomena, Munich, Germany.

Launder, B. E. and Sharma, B.I., (1974), Application of the energy dissipation model of turbulence to the calculation of flow near a spinning disc, Lett. Heat Mass Transfer, Vol. 1, pp. 131-138.

Masuda, S., Obi, S. and Aoki, K., (1994). Control of turbulent separating and reattaching flow by periodic perturbation, Turbulence Control, Vol. 193, pp. 55–61.

Raisee, M., (1999), Computation of flow and heat transfer through two- and three-dimensional rib-roughened passages, PhD. Thesis, UMIST.

Suga, K., (1996), Development and application of a non-linear eddy-viscosity model sensitised to stress and strain invariants, PhD. Thesis, Faculty of Technology, University of Manchester.